Color mixing from monolithically integrated InGaN-based light-emitting diodes by local strain engineering

Kunook Chung, Jingyang Sui, Brandon Demory, and Pei-Cheng Ku[a)]
Department of Electrical Engineering and Computer Science, University of Michigan, Ann Arbor, Michigan 48109, USA

(Received 27 April 2017; accepted 12 July 2017; published online 24 July 2017)

Additive color mixing across the visible spectrum was demonstrated from an InGaN based light-emitting diode (LED) pixel comprising red, green, and blue subpixels monolithically integrated and enabled by local strain engineering. The device was fabricated using a top-down approach on a metal-organic chemical vapor deposition-grown sample consisting of a typical LED epitaxial stack. The three color subpixels were defined in a single lithographic step. The device was characterized for its electrical properties and emission spectra under an uncooled condition, which is desirable in practical applications. The color mixing was controlled by pulse-width modulation, and the degree of color control was also characterized. *Published by AIP Publishing.*
[http://dx.doi.org/10.1063/1.4995561]

The light-emitting diode (LED) based microdisplay technology can meet the stringent demands for future augmented reality applications by providing the needed brightness, contrast, resolution, power efficiency, and device lifetime beyond the capabilities of current liquid crystal or organic LED display technologies.[1–5] Because LEDs are inherently monochromatic while displays require individually addressable red, green, and blue channels, attempts to realize an LED microdisplay typically involve assembly of three types of LED devices or selective deposition of different phosphor materials on a single-color LED pixel array.[6–8] Recently, various approaches have been introduced to enable monolithic integration of multi-color LED pixels on the same chip, which can potentially enable a higher spatial resolution and cut down the production cost. These methods include controlling and varying the indium composition using selective area epitaxy,[9–11] selective carrier injection into multiple quantum wells (MQWs) of different indium compositions,[12–14] and generating and controlling colors using local strain engineering.[15,16] Despite the initial successes of these monolithic approaches, color mixing has not been demonstrated. Color mixing is one of the key elements for any display technology. It requires independent and linear control of the intensity from each color channel. At the same time, the color coordinates of these color channels must remain stable. In this work, we present color mixing from a full-color LED pixel comprising three independent color channels, monolithically integrated on the same chip using local strain engineering.

The sample was grown on a 2 in. diameter c-plane sapphire substrate (unpatterned) by metal-organic chemical vapor deposition (MOCVD). The epitaxial structure consisted of five periods of $In_xGa_{1-x}N$/GaN MQWs. The indium composition and QW thickness were controlled such that the photoluminescence showed red ($\lambda \sim >600$ nm across the wafer) emission. A 20 nm-thick electron blocking layer of Mg-doped $Al_{0.2}Ga_{0.8}N$ was also inserted between the top layer of the MQWs and the Mg-doped p-GaN layer.

After growth, the red-green-blue (RGB) subpixels were fabricated as schematically shown in Fig. 1. The color generation mechanism is local strain engineering.[17–19] Blue and green colors were generated by locally relaxing the strain in the MQWs by using nanopillar structures, while the thin film structure itself was employed for the red color. The color is controllable by varying the nanopillar diameter. In this study, we chose 150 nm- and 50 nm-diameter nanopillars for the

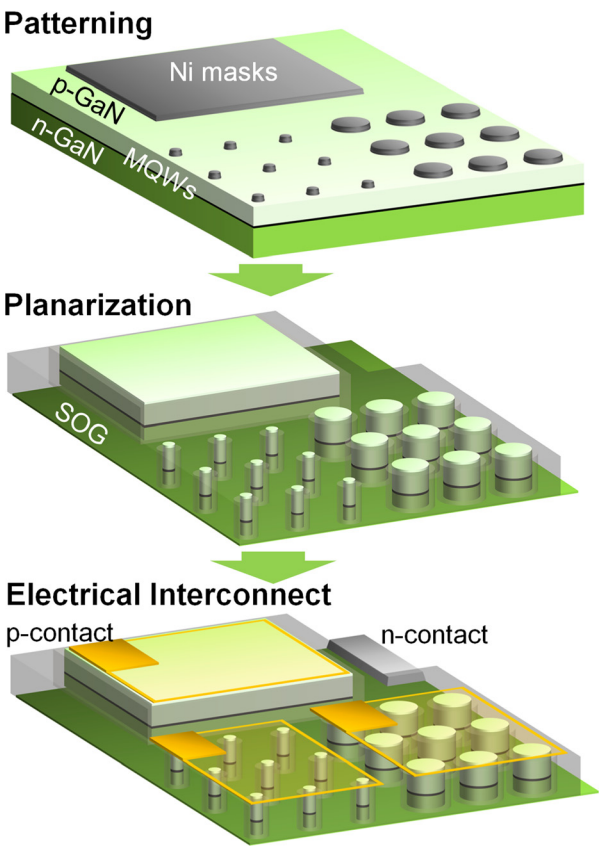

FIG. 1. Schematic of the fabrication process for the RGB LED pixel, which includes three steps: subpixel patterning, sample planarization, and formation of electrical interconnects.

[a)]Email: peicheng@umich.edu

green emission and blue emission, respectively. The fabrication process of the full-color LED pixel consisted of three major steps: the definition of nanopillar structures by lithography and etching, the planarization and electrical insulation, and the patterning of electrical interconnects. We used the same nickel mask to transfer and register the pattern between the steps. The details of the fabrication process are described elsewhere.[16,20]

The RGB color subpixels were designed such that their output intensities can be comparable for proper color mixing. In this study, the red emission was generated by a 400 μm $\times$ 400 μm thin-film LED. The green and blue emissions were generated from arrays of nanopillars. The green and blue subpixels consisted of 341×341 and 434×434 nanopillars, respectively. The spacing between two adjacent nanopillars was fixed at 300 nm for the ease of electron-beam lithography. In the future, it is possible to use interference or nanoimprint lithography to obtain a higher density of nanopillars. Moreover, the dimension of each pixel can be further decreased and is only limited by the diameter of each individual nanopillar as have been previously shown[19] and the electrical interconnects. Currently, the active region areas for the red, green, and blue subpixels were 160 000 μm^2, 2050 μm^2, and 370 μm^2, respectively. The distance between each subpixel was 150 μm. We have intentionally made the red subpixel area much larger to compensate for the low radiative efficiency due to the quantum-confined Stark effect (QCSE). It is possible to increase the efficiency of red emission, also by using nanopillar structures.[19] However, it will require a MQW active region with a longer ($\sim$650 nm) wavelength emission than what was available for the current experiment.

To generate color mixing, the RGB subpixels were biased at a fixed voltage modulated using a pulse-width modulation (PWM) scheme controlled by using a microcontroller (Arduino). The PWM allows the output intensity of the LED to be tuned without changing the emission wavelength. The sample was uncooled without any passive or active temperature control, a condition desirable for practical applications. All subpixels shared a common n-contact while they were individually addressed by separate p-contacts. The electrical characteristics of the nanopillar LEDs were reported elsewhere.[16] The output spectra were captured from the emission through the substrate using Ocean optics HR2000. The sapphire substrate was polished before the measurement for this purpose. We chose the voltages applied to the three subpixels to achieve comparable electroluminescence (EL) intensity outputs and the desired red emission wavelength. As shown in Fig. 2, the red emission experienced a strong QCSE with the increasing current density, while the blue and green emission wavelengths remained relatively constant. We chose a bias voltage for the red subpixel first such that its emission wavelength is $\gtrsim$600 nm. We then fixed a bias voltage for the blue and green subpixels such that they generated comparable output power as the red subpixel. In a microdisplay, the same bias voltage to all subpixels is desirable and can be achieved by fine tuning the ratios of the active region areas. However, the ability to adjust the intensity from the blue and green subpixels without changing their color coordinates greatly simplified the color mixing experiment presented below.

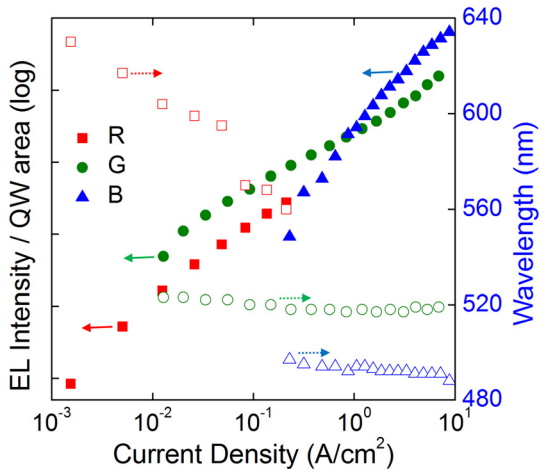

FIG. 2. The L-I characteristics and the peak emission wavelength of the RGB subpixels. Both the EL intensity and the current are normalized by the active region area of each subpixel.

Figure 3(a) shows light emission images from the RGB subpixels along with their spectra under different PWM duty cycles. We fixed the PWM frequency at 1 kHz and varied the pulse width from 100 μs to 900 μs. The frequency was sufficiently high that no light flickering was observable with the unaided eye. Meanwhile, we also observed some nonuniform intensity distributions within each subpixel, presumably because of the contact failures between the nanopillars and the thin (8/8 nm) Ni/Au bilayer in some local regions. However, we believe that this problem can be eventually solved by optimizing the fabrication process, such as using a sufficiently thick transparent conducting layer on the thin Ni/Au layer for more uniform current injection.

Figure 3(b) shows the EL spectra of the RGB subpixels at different PWM duty cycles. The bias voltages (and currents) were maintained at constant values as described above.

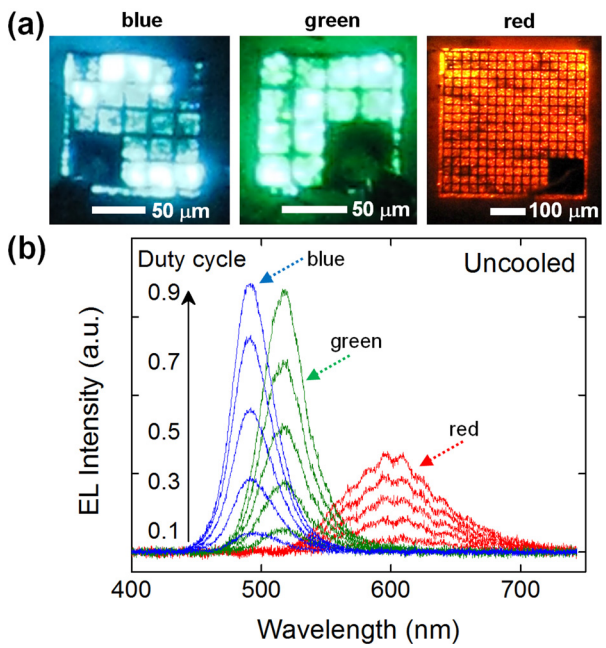

FIG. 3. (a) Microscopy images of the subpixels under bias. The grid lines are thick Ni/Au lines to help current spreading. (b) EL spectra of the RGB subpixels as a function of the PWM duty cycle varying from 0.1 to 0.9.

Only one dominant peak was observed for each spectrum. The dominant EL peaks were observed at 490 nm, 518 nm, and 600 nm for the blue, green, and red subpixels, respectively. When adjusting the duty cycle, the PWM maintained the color stability of all subpixels very well. At a 90% duty cycle, the ratios of the total output power from the RGB subpixels were measured at 1:1.3:1.3. As the green and blue pixels are relatively free from the QCSE due to the local strain relaxation in the InGaN/GaN MQW region, their EL wavelengths remained stable across a large range of injection current from 10^{-2} to 10 A/cm^2 (Fig. 2). Accordingly, we could balance the RGB pixels for color mixing by freely adjusting the injection current of the green and blue pixels to generate comparable intensity to that of the red pixel.

Figure 4(a) shows the color images and spectra of the color mixing results. Specifically, we obtained cyan and yellow colors using mixtures of blue and green and green and red, respectively. The corresponding EL spectra clearly show the combinations of each independent primary color emission. Furthermore, we investigated the linearity of color mixing from our device. Mainly, we wanted to verify that there was no crosstalk between subpixels when their duty cycles were independently tuned. Figure 4(b) shows the result on a CIE-1931 chromaticity diagram. We systematically varied the contributions from each subpixel according to a linear superposition and converted the measured spectrum into the CIE-1931 color coordinates. Ideally, these color coordinates should fall on lines connecting between the two end points on the color space, i.e., with one or two of the subpixels completely turned off. We represented these "ideal" cases using the dotted lines on the color space. The good agreement between the experimental data points (circle dots) and the theoretical curves (dotted lines) confirms the good linearity of our color mixing results. The color gamut covered by the current device is still smaller than desired for the display applications. In Fig. 4(b), we also show data obtained from the same sample, including 480 nm emission from a 40 nm nanopillar LED and 620 nm emission from a thin-film LED. These devices were not used in the color mixing experiment as they were not able to generate comparable output power as the rest of the devices. However, with further improvements of the epitaxial growth and optimization of the electrical properties for small-diameter nanopillar devices, it is expected that the color gamut can approach a typical organic LED display.[21,22]

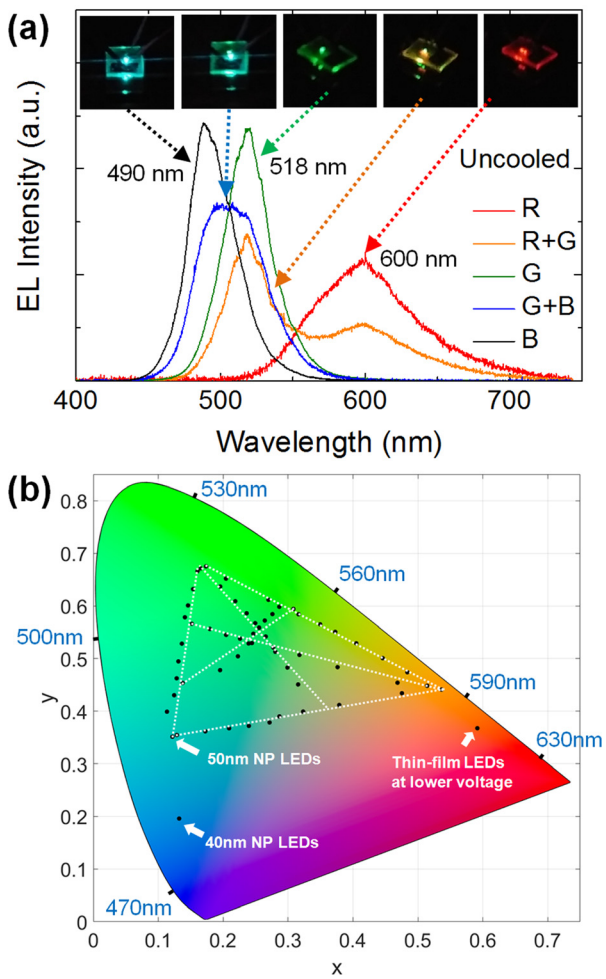

FIG. 4. Color mixing of the RGB subpixels. (a) EL spectra and the corresponding light emission images. (b) Each EL spectrum is converted into a set of CIE-1931 color coordinates. The white dotted lines correspond to the theoretical color mixing results expected from the two end points, i.e., with one or two of the color channels off for the case of two and three color mixing, respectively. Also shown are color coordinates of LED devices on the same sample which were not used in the color mixing experiment due to insufficient output power.

In summary, a potential LED color pixel suitable for the microdisplay application is shown. Both grayscale and color mixing were demonstrated with good linearity and controllability, even with an uncooled device. The fabrication used a top-down approach which is entirely compatible with the existing LED industrial infrastructure. Further improvements are still needed for optimal device performance. These include optimization of epitaxial growth of a longer ($\lambda \sim 650$ nm) wavelength LED structure, fabrication processes to yield better electrical properties for small-diameter nanopillar LEDs, and an improved design of the subpixel areas. Further reduction of the pixel size is also possible and achieves a high spatial resolution needed for near-to-eye display applications. Previously, we have shown good color control from submicron sized subpixels.[19] As a result, the proposed nanopillar LED devices can potentially provide a practical path for the future LED based microdisplay technology, especially aimed for augmented reality applications.

This work was supported by Samsung (N019887) for growth, fabrication, and device design and the National Science Foundation (DMR 1409529) for the studies of optical properties. We thank Professor Hui Deng from the University of Michigan and her group for fruitful discussions.

[1]F. A. Ponce and D. P. Bour, Nature **386**, 351 (1997).
[2]Z. Y. Fan, J. Y. Lin, and H. X. Jiang, J. Phys. D: Appl. Phys. **41**, 094001 (2008).
[3]S. Zhang, Z. Gong, J. J. D. McKendry, S. Watson, A. Cogman, E. Xie, P. Tian, E. Gu, Z. Chen, G. Zhang, A. E. Kelly, R. K. Henderson, and M. D. Dawson, IEEE Photonics J. **4**, 1639 (2012).
[4]Z. J. Liu, W. C. Chong, K. M. Wong, K. H. Tam, and K. M. Lau, IEEE Photonics Technol. Lett. **25**, 2267 (2013).
[5]F. Templier, J. Soc. Inf. Disp. **24**, 669 (2016).
[6]E. F. Schubert and J. K. Kim, Science **308**, 1274 (2005).
[7]Y. Huang, X. Duan, and C. M. Lieber, Small **1**, 142 (2005).

[8]T.-H. Kim, K.-S. Cho, E. K. Lee, S. J. Lee, J. Chae, J. W. Kim, D. H. Kim, J.-Y. Kwon, G. Amaratunga, S. Y. Lee, B. L. Choi, Y. Kuk, J. M. Kim, and K. Kim, Nat. Photonics **5**, 176 (2011).
[9]K. Kishino, K. Nagashima, and K. Yamano, Appl. Phys. Express **6**, 12101 (2013).
[10]R. Wang, H. P. T. Nguyen, A. T. Connie, J. Lee, I. Shih, and Z. Mi, Opt. Express **22**, A1768 (2014).
[11]Y. H. Ra, R. J. Wang, S. Y. Woo, M. Djavid, S. M. Sadaf, J. Lee, G. A. Botton, and Z. Mi, Nano Lett. **16**, 4608 (2016).
[12]Y. J. Hong, C.-H. Lee, A. Yoon, M. Kim, H.-K. Seong, H. J. Chung, C. Sone, Y. J. Park, and G.-C. Yi, Adv. Mater. **23**, 3284 (2011).
[13]H. P. T. Nguyen, K. Cui, S. Zhang, S. Fathololoumi, and Z. Mi, Nanotechnology **22**, 445202 (2011).
[14]H. S. El-Ghoroury, M. Yeh, J. C. Chen, X. Li, and C.-L. Chuang, AIP Adv. **6**, 075316 (2016).
[15]Y.-J. Lu, H.-W. Lin, H.-Y. Chen, Y.-C. Yang, and S. Gwo, Appl. Phys. Lett. **98**, 233101 (2011).
[16]K. Chung, J. Sui, B. Demory, C.-H. Teng, and P.-C. Ku, Appl. Phys. Lett. **110**, 111103 (2017).
[17]Y. Kawakami, A. Kaneta, L. Su, Y. Zhu, K. Okamoto, M. Funato, A. Kikuchi, and K. Kishino, J. Appl. Phys. **107**, 023522 (2010).
[18]L. Zhang, L.-K. Lee, C.-H. Teng, T. A. Hill, P.-C. Ku, and H. Deng, Appl. Phys. Lett. **104**, 051116 (2014).
[19]C.-H. Teng, L. Zhang, H. Deng, and P.-C. Ku, Appl. Phys. Lett. **108**, 071104 (2016).
[20]L. Zhang, C.-H. Teng, P.-C. Ku, and H. Deng, Appl. Phys. Lett. **108**, 153102 (2016).
[21]M. C. Gather, A. Köhnen, A. Falcou, H. Becker, and K. Meerholz, Adv. Funct. Mater. **17**, 191 (2007).
[22]C.-H. Chang, H.-C. Cheng, Y.-J. Lu, K.-C. Tien, H.-W. Lin, C.-L. Lin, C.-J. Yang, and C.-C. Wu, Org. Electron. **11**, 247 (2010).